22nd International Conference on Renewable Energies and Power Quality (ICREPQ'24)
Bilbao (Spain), 26th to 28th June 2024

ISBN: 978-84-09-60656-6

Influence of tin addition to Al-3%Mg (wt.%) alloys for hydrogen generation

L. Giovanetti[1], A.V. Rodrigues[1,2], R. Kakitani[1], C. Silva[1], C. Brito[3], P.R. Mei[1,4], A. Garcia[1], N. Cheung[1]

[1] Department of Manufacturing and Materials Engineering, University of Campinas, 13083-860 Campinas, SP, Brazil
Phone number: +55 19 3521 3309

[2] Federal Institute of Education, Science and Technology of São Paulo, 12903-000 Bragança Paulista, SP, Brazil
Phone number: +55 11 4034-7800

[3] Department of Aeronautical Engineering/School of Engineering, São Paulo State University, 13876-750 São João da Boa Vista, SP, Brazil, Phone number: +55 19-3638-2400

[4] Federal Institute of Education, Science and Technology of São Paulo, IFSP, 01109-010, São Paulo, SP, Brazil
Phone number: +55 11 2763-7568

Abstract. Global attention is increasingly focused on recycling and clean energy generation. The present study delves into both areas by examining the reuse of secondary aluminium for hydrogen generation. The aim is to investigate how the microstructural length scale influences the hydrogen production behaviour of two Al-3%Mg (wt.%) alloys, with and without a 10% Sn addition. Al-3%Mg serves as base for commercial alloys like 5056, 5154, and 5754. Additionally, since Sn is normally used as a solid lubricant for bearings, the analysis also extends to Sn-containing Al-Mg alloys, which can be repurposed for clean energy generation, after the end of their life service. Solidified samples with varying microstructural length scales underwent hydrogen evolution tests in a 1 M NaOH solution. While the binary alloy shows no sensitivity with respect to the microstructural length scale in hydrogen production rate, Sn not only exhibits sensitivity but also boosts it by approximately 350 % when both alloys are compared.

Key words. Solidification, Hydrogen generation, microstructure.

1. Introduction

Hydrogen is considered one of the potential future energy sources due to its high enthalpy of combustion (releasing twice more energy than gasoline [1]) and its production of clean reaction products (just water and energy). However, the current methods for hydrogen production mostly rely on fossil fuels, such as steam methane reforming and partial methane oxidation [2], both of which release greenhouse gases.

As an alternative, the hydrolysis of aluminium holds great potential for cleaner hydrogen production. Typically, sodium hydroxide is introduced to water, accelerating the chemical reaction, with the resulting corrosion products being hydrogen gas and aluminium hydroxides. Then, the hydrogen can be processed and used as fuel, while the hydroxide can be reused for other applications (such as alumina and primary aluminium production [3,4]).

The great availability, low density, and high hydrogen storage capacity make Al stand out compared to other metals [5,6]. However, the surface passivation of Al makes the corrosion process more difficult, thereby decreasing the rate of hydrogen generation. The addition of Sn to Al offers a potential solution to enhance hydrolysis reactions. As an immiscible element, Sn segregates to the boundaries and promotes higher reactivity with the α-Al matrix [7-9].

Another step toward eco-friendly H_2 production involves the possibility of using waste Al alloys instead of primary aluminium. With the enhancement of hydrolysis kinetics through Sn addition [10], Al recycling can be achieved by incorporating Sn during the remelting of Al scraps or reusing Sn-containing Al alloys without remelting after their life service. Compared to primary production, Al recycling demands 95% less energy and emits 5% of the greenhouse gas [11], resulting in significantly lower environmental impact. One of the potential options are Al-Mg alloys (5xxx series), employed in the marine industry, automobile parts, packing, and structural components [12,13], and Al-Mg-Sn alloys (base for bearing materials [14]). While the hydrolysis of Al-Mg is relatively known in the literature [15], there are currently no reports on H_2 generation using Al-Mg-Sn alloys.

Besides the chemical composition, the microstructure of the alloys plays a significant role in the H_2 generation rate, i.e., a fast hydrolysis reaction can be achieved through the control of the degree of microstructure refinement [7]. Therefore, this study compares the H_2 generation during the hydrolysis of an Al-3%Mg (base for the 5056, 5154 and 5754 commercial alloys [16]) and Al-3%Mg-10%Sn

alloys, evaluating the effects of Sn and the microstructure refinement. The alloys were solidified under different cooling rates, producing coarse and fine microstructures, and the H_2 generation rate was correlated with a microstructural parameter.

2. Experimental procedure

An Al-10%Sn-3%Mg (wt.%) alloy was prepared using commercially pure metals, whose compositions are summarized in Table 1. Initially, Al, placed in an alumina-coated silicon carbide (SiC) crucible, was melted in a resistance furnace. The Al liquid bath was overheated about 150 °C. After adding Sn and Mg pieces to the bath, they were mechanically mixed and stirred with argon (Ar) for 10 minutes, to degas and achieve homogeneity. The crucible was returned into the furnace until the aforementioned overheating was attained. This procedure was repeated 03 times to ensure proper homogenization. Subsequently, the molten alloy was poured into a cylindrical stainless steel split mold, with its inner surfaces previously coated with an alumina layer to minimize radial heat losses. The bottom part of the mold was closed with a 3 mm thick AISI 1020 carbon steel sheet. A vertical upward directional solidification was promoted using a water-cooled directional solidification apparatus, in which the mold containing the alloy was positioned. The alloy was reheated around 20 ºC above the alloy *liquidus* temperature. Then, the electric heaters were immediately switched off and the water flow at the bottom part of the mold was started. During the solidification process, the temperature was continuously monitored using 8 (eight) fine K-type thermocouples located at different positions along the length of the casting. A data logger system was used to record the temperature profiles, at a frequency of 20 Hz. Figure 1 displays a schematic representation of the solidification apparatus.

Table I. Chemical composition (wt %) of metals used to prepare the Al-Sn-Mg alloy

Element	Al	Cu	Mg	Zn	Si	Sn	Ni	Mn	Fe	Pb
Al	balance	0.01	0.01	0.01	0.03	-	-	-	0.03	-
Sn	0.0006	0.0004	-	0.002	-	balance	0.0001	-	0.0025	0.001
Mg	6.981	0.115	balance	0.631	0.138	0.005	0.001	0.139	0.001	-

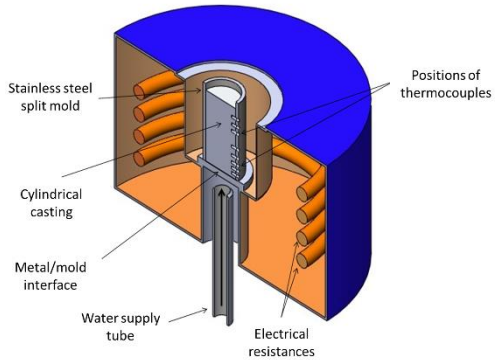

Fig. 1. Schematic representation of water-cooled upward directional solidification apparatus.

The longitudinal and transverse microstructures were assessed from samples extracted at positions (P) 5, 10, 15, 20, 25, 30, 40, 50, 60 and 70mm from the metal/mold interface (cooled surface of the casting) along the length of the directionally solidified (DS) casting. These samples were ground with silicon carbide papers from 100 to 1200 mesh and polished using diamond paste (1 and 3 µm). No chemical etching was required to reveal the microstructure, indicating that the alloy is reactive solely through polishing. The images of dendritic microstructures were acquired through an Olympus Inverted Metallurgical Microscope (model 41GX) and the triangle method [17] was employed to measure the primary dendritic arm spacings (λ_1). At least 40 measurements were performed for each selected position (P). Intermetallic compounds (IMCs) were analysed by a Scanning Electron Microscope (SEM) (Inspect F50) coupled with an energy dispersive X-ray spectrometer (EDS) (Oxford-X-MAX). The solidification thermal parameters and the microstructural growth of a directionally solidified Al-3%Mg (wt.%) alloy were previously examined by Brito and coauthors [18]. In the present study, in addition to a comparison of these results with those obtained for the Al-10%Sn-3%Mg alloy, both alloys underwent hydrogen evolution tests. A full immersion hydrogen testing assembly was utilized for hydrogen evolution measurements at room temperature (25 ± 2 °C). This experimental apparatus, developed based on gravimetric principles, conducted the hydrogen evolution of both alloys in a 1M NaOH solution.

To monitor the hydrogen production, the sample was directly fixed in a fully immersed container, and the entire system was coupled to a high-precision balance. The cylindrical samples were machined with a diameter of 8 mm (0.5 cm² of area) and a height of 5 mm. Before testing, specimens, relative to the microstructure length scale of interest, were cold-mounted using a polyester resin (type 1.0#0.8, Arazin) exposing only the 0.5 cm² area to the NaOH solution. Schematic representations of the experimental apparatus and samples are presented in Figure 2.

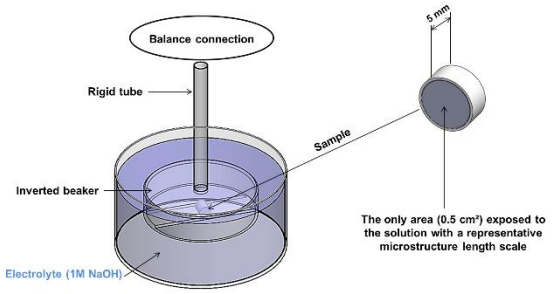

Fig. 2. Schematic representation of the apparatus used for measuring of hydrogen released and samples for hydrogen evolution tests.

As the Al-Sn-Mg samples dissolve, the generated H_2 rises to the top of the container, altering the weight displayed on the balance. This change results from the variation in the buoyant force produced due to the volume of solution displaced by the evolved H_2. All the hydrogen evolution tests were conducted in triplicate.

3. Results and discussion

Figure 3 shows the partial Al-(0-20)%Sn-3%Mg phase diagram, generated using the JMatPro v.13.2 software. As can be observed, a dashed line indicates the composition of the ternary alloy investigated in this work: Al-10%Sn-3%Mg. The expected phases are α-Al, Mg_2Sn and β-Sn, respectively named as AL, MG2X_C1 and SN in the diagram.

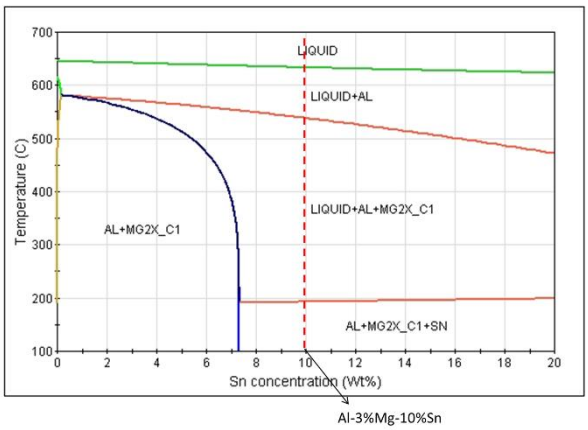

Fig. 3. Partial phase diagram of the Al-(0-20)%Sn-3%Mg system with the dashed line indicating the analysed alloy composition (JMatPro v.13.2).

The cooling curves obtained from the thermocouples positioned along the DS casting are presented in Figure 4. These thermal profiles were analysed and allowed the determination of the solidification thermal parameters: growth rate (V_L) and cooling rate ($\dot{T}$) concerning the *liquidus* isotherm. The cooling rate curves were obtained from the time-derivative of $T=f(t_L)$, where t_L is the time when the liquidus isotherm passed through a given position P from the bottom of the DS casting. Both thermal parameters are presented in Figure 5.

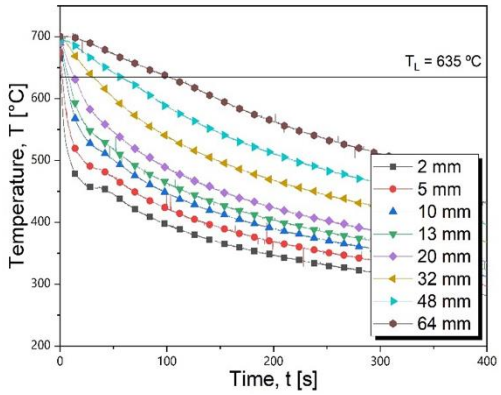

Fig. 4. Thermal profiles in the DS Al-10%Sn-3%Mg alloy casting for several thermocouples' positions.

In Figure 5, when comparing the ternary alloy of this work to the results obtained by Brito and co-authors [18] for a DS Al-3%Mg alloy, the addition of Sn is found to increase the cooling rates. Concerning the growth rates, higher V_L values are observed for the ternary alloy casting up to approximately P = 25 mm, beyond which the binary alloy begins to exhibit higher values. Two representative microstructures observed at transverse sections of the Al-10%Sn-3%Mg alloy are shown in Figure 6. The Al-rich matrix containing a dendritic morphology prevailed along the entire DS casting. The microstructure gradually becomes coarser with the increasing distance from the metal/mold interface. This result stems from both the increasing thermal resistance imposed by the continuous growth of the solidified layer and the increasing metal/mold interfacial thermal resistance that occurs during the evolution of the solidification process. Murty and coauthors [19] reported that the increase in cooling rates, the addition of solute elements, and inoculation are the main ways of achieving microstructural refinement during solidification.

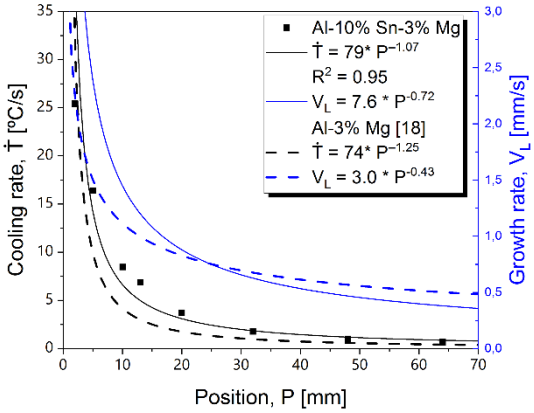

Fig. 5. Profiles of V_L and $\dot{T}$ as a function of position (P) from the cooled bottom of the DS Al-10%Sn-3%Mg alloy casting.

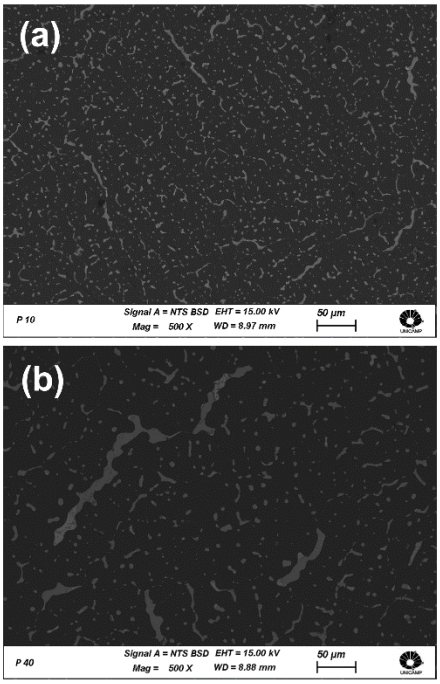

Fig. 6. Transverse images obtained by SEM for (a) 10 mm and (b) 40 mm positions from the water-cooled surface of the DS Al-10%Sn-3%Mg alloy casting.

The evolution of the primary dendrite arm spacing (λ_1), its mean values and range of maximum and minimum experimental values of the DS Al-10%Sn-3%Mg alloy casting are presented in Figure 7. The average values of λ_1 are related to the cooling ($\dot{T}$) and growth rates respectively by the experimental laws: $\lambda_1 = 92\dot{T}^{-0.55}$ and $\lambda_1 = 39V_L^{-1.1}$.

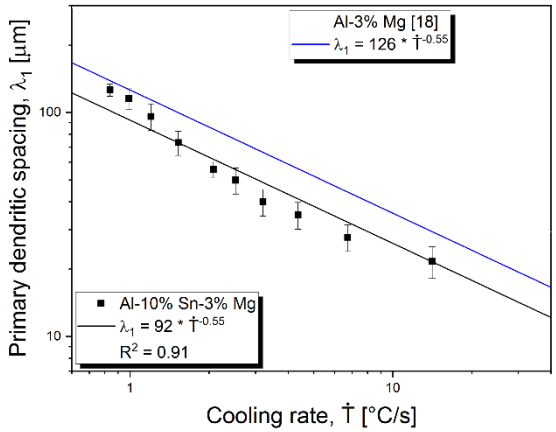

Fig. 7. Primary dendrite arm spacing λ_1 along the length of the DS Al-10%Sn-3%Mg alloy casting as a function of cooling rate.

Figure 8 show elemental SEM-EDS analysis (punctual) of the DS Al-10%Sn-3%Mg alloy. Intermetallic compounds (IMCs) are evident in the interdendritic regions, while a rich-Al matrix contains low amounts of Mg and Sn. The quantity of Mg exceeds that of Sn (point 3) due to its higher solubility in Al. A difference of image contrasts is observed within the IMCs. The phase with higher Sn content (with a maximum of 0.02wt.%Mg at point 2) appears lighter than the phase with a greater concentration of Mg (28.11wt.% - point 1). This contrast difference can be explained by the higher atomic number of Sn (50) compared to that of Mg (12). Different phases exhibit distinct BSE (backscattered electrons) emission coefficient (η) and target atomic number (Z), which implies in images containing different intensities and contrasts [20]. As predicted in the partial phase diagram presented in Figure 3, the brighter IMC is likely the β-Sn phase, commonly referred to as "White tin" [21]. An EDS analysis of the grey phase revealed a proportion close to 30wt.%Mg and 70wt.%Sn, aligning with the stoichiometry of Mg_2Sn phase, indicating its formation. Concerning the phase diagram of the binary Al-Mg system, it is expected the formation of α-Al and Al_3Mg_2 phases for the aforementioned composition [22], which were also observed in the present work.

Figure 9 shows the first-time derivative (flow rate) of hydrogen evolution curves of Al-10%Sn-3%Mg and Al-3%Mg alloys immersed in a 1 M/L NaOH aqueous solution. Each point represents the mean value obtained from tests carried out in triplicate. For the ternary alloy (Al-10%Sn-3%Mg) five positions, with different microstructure length scales were analysed while for the binary alloy (Al-3%Mg alloy), three positions. Analysing the binary alloy (Al-3%Mg alloy), all flow rate profiles are relatively closer to each other and changes in the microstructure length scale seems not to accelerate or decelerate the hydrogen generation, which remains close to 0.26 mL/(cm².min).

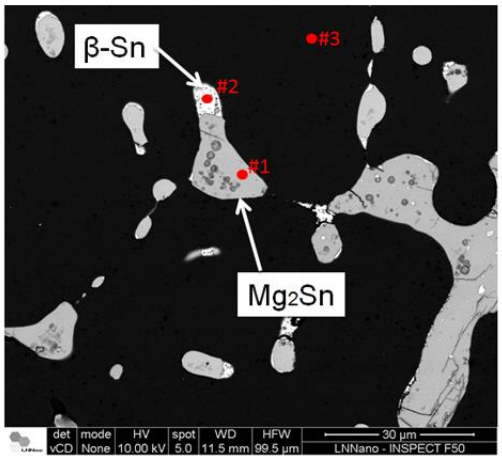

Point	Al (wt.%)	Mg (wt.%)	Sn (wt.%)
#1	0.39	28.11	71.50
#2	0.64	0.02	99.34
#3	98.95	0.97	0.07

Fig. 8. Elemental SEM-EDS analyses in a transverse section of the DS Al-10%Sn-3%Mg alloy casting.

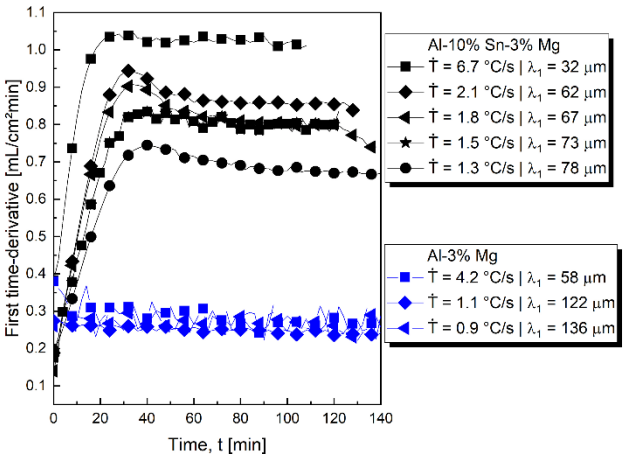

Fig. 9. Hydrogen flow rate for different microstructure length scales (λ_1) of Al-10%Sn-3%Mg and Al-3%Mg alloys.

Contrary to what can be observed for the Al-3%Mg alloy, for the alloy containing Sn, there is a clear tendency for acceleration of hydrogen generation with the refinement of the microstructure. The sample with a lower λ_1 (solidified under $\dot{T}$ = 6.7 °C/s) presents a hydrogen flow rate near of 1.05 mL/(cm².min). This flow rate decreases with the coarsening of the microstructure until reaching 0.7 mL/(cm².min), observed at the position with the highest λ_1 (λ_1 = 78 μm). It is worth mentioning that the most refined microstructure of the binary alloy (λ_1 = 58 μm) presents a hydrogen flow rate which is less than half of the flow rate of the coarser microstructure of the alloy with Sn addition (λ_1 = 78 μm).

In a recent study on the corrosion behaviour of Al-3%Mg, Al-5%Mg and Al-7%Mg alloys in a 3.5wt. %NaCl medium, Haque and coauthors [23] reported that the intermetallic phase of Al_2Mg_3 acts as an anode in a micro-

galvanic couple and is corroded. However, there is a formation of a protective and stable surface layer of Al_2O_3, leading to a steady corrosion rate after a short period of exposure to the aqueous medium. This explains the low hydrogen release rates throughout the testing period even supressing the possible influence of the different microstructural scales on the hydrogen flow rate since the results remained stable and practically at the same value for all positions analysed along the length of the DS casting (Figure 9).

To improve reactivity and, consequently, boost the rate of hydrogen production, researchers have suggested incorporating certain chemical elements, particularly those with low melting points [24]. Examples of such elements include Sn, Zn, In, and Ga. These elements play a role in preventing the formation of a passive layer and altering the corrosion potential of the alloy towards more negative values [25]. Additionally, according to Song and Shi [26] the Mg_2Sn phase acts an initiation site for pitting corrosion, increasing the corrosion rate. Thus, the presence of not only the Mg_2Sn IMC but also of β-Sn particles in theAl-10%Sn-3%Mg alloy promotes higher hydrogen flow rates when compared to those of the Al-3%Mg alloy in which these phases are absent. The different hydrogen flow rates observed among the analysed range of λ_1 values of the DS Al-10%Sn-3%Mg alloy casting seem to be mainly associated with the better distribution of IMCs and β-Sn particles in more refined microstructures. The Mg_2Sn and β-Sn particles serve as cathodes and thus favour the dissolution of the α-Al phase increasing the hydrogen flow rates for lower values of λ_1.

The presented first time-derivatives of the hydrogen evolution curves represents the hydrogen flow rate (ϕ), which varies with time and has different profiles (depending on the alloy). Therefore, it is more adequate to present the average flow rate of hydrogen (ϕ_{ave}). This will allow proper comparisons among the investigated alloys of this work. The average flow rate was obtained by the following equation:

$$\phi_{ave} = \frac{1}{t_0 - t_{test}} \int_{t_0}^{t_{test}} \phi(t)dt \qquad (1)$$

where: t_0 and t_{test} means upper and lower limits of the ϕ domain, respectively, and (t_{test} - t_0) corresponds to the total test time).

Figure 10 shows ϕ_{ave} for the studied alloys immersed in a 1 M/L NaOH aqueous solution. The alloy containing Sn present higher values of ϕ_{ave} compared to those of the binary Al-Mg alloy, proving the beneficial effect of Sn for hydrogen generation. In the ternary alloy, the generation of hydrogen is sensitive to variations in the microstructure length scale. i.e. ϕ_{ave} decreases with the increase in λ_1. For the binary alloy ϕ_{ave} remains almost the same along the length of the DS casting.

Figure 11 shows a SEM image of the microstructure of the Al-10%Sn-3%Mg alloy after 40 minutes of hydrogen evolution tests. Pitting corrosion starts at the interface of the Al-rich matrix (dendrites) and the IMCs (Mg_2Sn and β-Sn), with these IMCs acting as cathodes during the electrochemical process. The increase in testing duration intensifies the pitting corrosion, leading to progressive consumption of the Al-rich matrix. Sn promoted the increase in α-Al hydrolysis, leading to faster hydrogen production in the ternary alloy as compared to that of the binary alloy. In a recent study [27], an investigation about H_2 generation in an Al-1%Fe-9%Sn, revealed the same dissolution pattern observed around both the Sn particles and the Fe-containing IMCs.

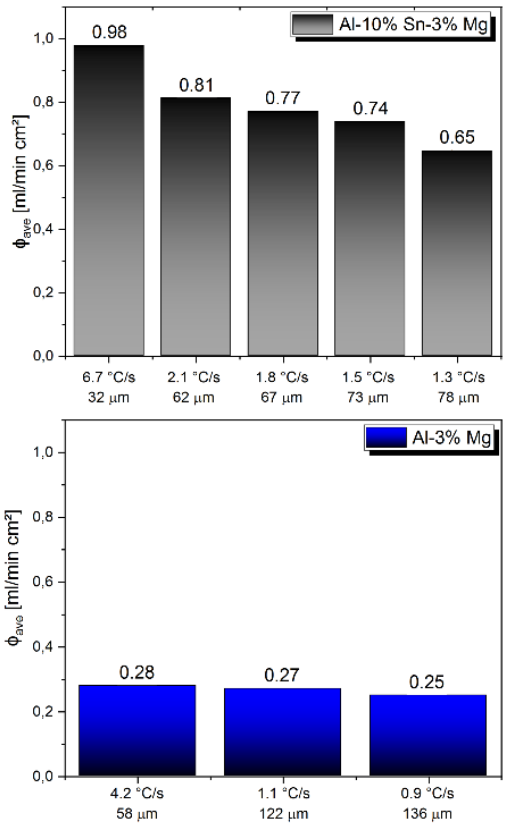

Fig. 10. ϕ_{ave} for Al-10%Sn-3%Mg and Al-3%Mg alloys.

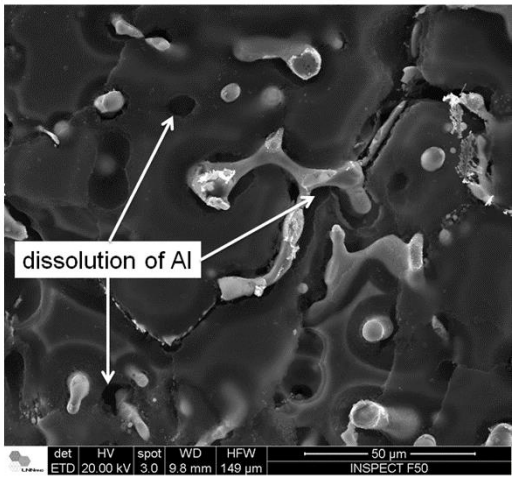

Fig. 11. SEM image showing the microstructural changes in the Al-10%Sn-3%Mg alloy after 40 minutes of hydrogen evolution tests.

4. Conclusion

From this investigation, the following conclusions can be drawn:

The hydrogen generation rate for the Al-3%Mg alloy showed low sensitivity to microstructural variation, averaging about 0.26 ml/**(**cm².min**)**. In contrast, the microstructural refinement achieved in the Al-3%Mg-10%Sn alloy through variations in the cooling regime during solidification induced a remarkable 350% increase (0.98 ml/**(**cm².min**)**) in hydrogen production as compared to that of the Al-3%Mg alloy. These results shows that secondary aluminium can be a potential source for clean energy generation.

Acknowledgement

This work was supported by CNPq—National Council for Scientific and Technological Development (Grants 407871/2018-7, 303140/2020-8, 308825/2021-7, 140180/2022-2 and 383551/2022-6); FAPESP—São Paulo Research Foundation, Brazil (Grant: 2021/11439-0) and FAEPEX/UNICAMP-Fundo de Apoio ao Ensino, à Pesquisa e à Extensão (Grants 2162/21 and 2549/22). This research used the facilities of the Brazilian Nanotechnology National Laboratory (LNNano), part of the Brazilian Centre for Research in Energy and Materials (CNPEM). The SEM-FIB staff is acknowledged for their assistance during the analyses (SEM-FIB-C1-20210602).

References

[1] G. Marbán and T. Valdés-Solís, "Towards the hydrogen economy?", International Journal of Hydrogen Energy (2007). Vol. 32, pp. 1625-1637.

[2] B.E. Lebrouhi, J.J. Djoupo, B. Lamrani, K. Benabdelaziz and T. Kousksou, "Global hydrogen development – A technological and geopolitical overview", International Journal of Hydrogen Energy (2022). Vol. 47, pp. 7016-7048.

[3] C. Misra, Kirk-Othmer Encyclopedia of Chemical Technology, Wiley, Hoboken (2001), p. 421-433.

[4] S. Yang and H. Knickle, "Design and analysis of aluminum/air battery system for electric vehicles", Journal of Power Sources (2002). Vol. 112, pp. 162-173.

[5] C.-Y. Ho and C.-H. Huang, "Enhancement of hydrogen generation using waste aluminum cans hydrolysis in low alkaline de-ionized water", International Journal of Hydrogen Energy (2016). Vol. 41, pp. 3741-3747.

[6] H.Z. Wang, D.Y.C. Leung, M.K.H. Leung and M. Ni, "A review on hydrogen production using aluminum and aluminum alloys", Renewable and Sustainable Energy Reviews (2009). Vol. 13, pp. 845-853.

[7] C. Konno, C. Cruz, T. Costa, A. Barros, P. Goulart, A. Garcia and N. Cheung, "Solidification microstructure-dependent hydrogen generation behavior of Al-Sn and Al-Fe alloys in alkaline medium", International Journal of Hydrogen Energy (2021). Vol. 46, pp. 12654-12671.

[8] Y. Liu, X. Liu, X. Chen, S. Yang and C. Wang, "Hydrogen generation from hydrolysis of activated Al-Bi, Al-Sn powders prepared by gas atomization method", International Journal of Hydrogen Energy (2017). Vol. 42, pp. 10943-10951.

[9] H.A El Shayeb, F.M Abd El Wahab and S Zein El Abedin, "Electrochemical behaviour of Al, Al-Sn, Al-Zn and Al-Zn-Sn alloys in chloride solutions containing stannous ions", Corrosion Science (2001). Vol. 43, pp. 655-669.

[10] K. Eom, M. Kim, S. Oh, E. Cho and H. Kwon, "Design of ternary Al–Sn–Fe alloy for fast on-board hydrogen production, and its application to PEM fuel cell", International Journal of Hydrogen Energy (2011). Vol. 36, pp. 11825-11831.

[11] S. Capuzzi and G. Timelli, "Preparation and Melting of Scrap in Aluminum Recycling: A Review", Metals (2018). Vol. 8, pp. 249.

[12] D. Zhou, X. Zhang, H. Wang, Y. Li, B. Sun and D. Zhang, "Influence of Mg on tensile deformation behavior of high Mg-content Al-Mg alloys", International Journal of Plasticity (2022). Vol. 157, pp. 103405.

[13] G. Yi, D.A. Cullen, K.C. Littrell, W. Golumbfskie, E. Sundberg and M.L. Free, "Characterization of Al-Mg Alloy Aged at Low Temperatures", Metallurgical and Materials Transactions A (2017). Vol. 48, pp. 2040-2050.

[14] M. Sadawy, H. Metwally, H.A. El-Aziz, A. Adbelkarim, W. Mohrez, H. Mashaal and A. Kandil, "The role of Sn on microstructure, wear and corrosion properties of Al-5Zn-2.5Mg-1.6Cu-xSn alloy", Materials Research Express (2022). Vol. 9, pp. 096507.

[15] W. Yang, T. Zhang, J. Zhou, W. Shi, J. Liu, K. Cen, "Experimental study on the effect of low melting point metal additives on hydrogen production in the aluminum-water reaction", Energy (2015), Vol. 88, p. 537-543.

[16] K. Anderson, J. Weritz and J.G. Kaufman, Properties and Selection of Aluminum Alloys, Materials Park, ASM International, (2019), pp. 1-636.

[17] M. Gündüz and E. Çadırlı, "Directional solidification of aluminium–copper alloys", Materials Science and Engineering: A (2002). Vol. 327(2), pp. 167-185.

[18] C. Brito, F. Bertelli, M.A.P. Castanho, P.R. Goulart, N. Cheung, J.E. Spinelli and A. Garcia, "Upward and downward unsteady-state directional solidification of a hypoeutectic Al-3wt.%Mg alloy", Ciência & Tecnologia dos Materiais (2017). Vol. 29(1), pp. e65-e70.

[19] B.S. Murty, S.A. Kori and M. Chakraborty, "Grain refinement of aluminium and its alloys by heterogeneous nucleation and alloying", International Materials Reviews (2002). Vol. 47(1), pp .3-29.

[20] G.E. Lloyd, "Atomic number and crystallographic contrast images with SEM: A review of backscattered electron techniques", Mineralogical Magazine (1987). Vol. 51, pp. 3-19.

[21] S-H. Na and C-H. Park, "First-Principles Study of the Structural Phase Transition in Sn", Journal of the Korean Physical Society (2010). Vol. 56(1), pp. 494-497.

[22] H. Okamoto, "Al-Mg (aluminum-magnesium)", Journal of Phase Equilibria (1998). Vol. 19, pp. 598.

[23] M.S. Haque, M. Nomani, A. Akter and I.A. Ovi, "Synergistic effect of Mg addition on the enhancement of the mechanical properties and evaluation of corrosion behaviors in 3.5 wt.% NaCl of Aluminum Alloys", Heliyon (2024) in press. doi: https://doi.org/10.1016/j.heliyon.2024.e25437

[24] S.P. Du Preez and D.G. Bessarabov, "The effects of bismuth and tin on the mechanochemical processing of aluminum-based composites for hydrogen generation purposes", International Journal of Hydrogen Energy (2019). Vol. 44, pp. 21896–21912.

[25] S. Khireche, D. Boughrara, A. Kadri, L. Hamadou and N. Benbrahim, "Corrosion mechanism of Al, Al–Zn and Al–Zn–Sn alloys in 3wt.% NaCl solution", Corrosion Science (2014). Vol. 87, pp. 504-516.

[26] G-L. Song and Z. Shi, "Corrosion mechanism and evaluation of anodized magnesium alloys", Corrosion Science (2014). Vol. 85, pp. 126-140.

[27] A. Barros, C. Konno , A. de Paula, C. Silva, A. Garcia, N. Cheung, "The role of microstructural length scale in hydrogen generation features of an Al-Sn-Fe alloy", Metals (2024). Vol.14, pp. 187.